Journal of the Optical Society of America A
OPTICS, IMAGE SCIENCE, AND VISION

Analyzing the relationship between decorrelation time and tissue thickness in acute rat brain slices using multispeckle diffusing wave spectroscopy

JOSHUA BRAKE,*,† MOOSEOK JANG,† AND CHANGHUEI YANG

Department of Electrical Engineering, California Institute of Technology, Pasadena, California 91125, USA
**Corresponding author: jbrake@caltech.edu*

Received 6 October 2015; revised 4 December 2015; accepted 26 December 2015; posted 5 January 2016 (Doc. ID 251465); published 1 February 2016

Novel techniques in the field of wavefront shaping have enabled light to be focused deep inside or through scattering media such as biological tissue. However, most of these demonstrations have been limited to thin, static samples since these techniques are very sensitive to changes in the arrangement of the scatterers within. As the samples of interest get thicker, the influence of the dynamic nature of the sample becomes even more pronounced and the window of time in which the wavefront solutions remain valid shrinks further. In this paper, we examine the time scales upon which this decorrelation happens in acute rat brain slices via multispeckle diffusing wave spectroscopy and investigate the relationship between this decorrelation time and the thickness of the sample using diffusing wave spectroscopy theory and Monte Carlo photon transport simulation.

OCIS codes: (290.4210) Multiple scattering; (290.7050) Turbid media; (290.5820) Scattering measurements.

http://dx.doi.org/10.1364/JOSAA.33.000270

1. INTRODUCTION

The optical opacity of biological tissue in the visible regime has long been a challenge in the field of biomedical optics. Since the light traveling through thick samples undergoes many scattering events, the information about the sample is scrambled and the light field exiting the sample forms a random speckle pattern [1].

While this scrambling of the light field makes it difficult to accurately image thick, highly scattering biological samples with conventional optical techniques, new research in the field of wavefront shaping enables light to be focused in or through strongly scattering tissue and has demonstrated progress toward this goal of deep-tissue imaging [2–6]. In contrast to techniques such as confocal microscopy or optical coherence tomography, which seek to gate out and use only the unscattered or singly scattered portion of light passing through the sample, these wavefront shaping techniques incorporate even multiply scattered portions of the scattered light field.

While these wavefront shaping techniques have been primarily demonstrated with static scattering samples or fixed biological tissues, the ability to apply these techniques to living biological tissues is the ultimate goal. The main challenge facing this development is the dynamic nature of living tissue. In biological tissue where the average number of scattering events for an individual photon traveling through the sample is very large, small changes in the composition of the sample can break the time-reversal symmetry of optical scattering and cause a mismatch between the shaped wavefront and the correct wavefront solution, severely degrading the quality of the shaped focus. From previous studies, it is known that this degradation is proportional to the intensity autocorrelation function of the scattered light—a conventional measure of scatterer movement [7].

In this study, we measure the intensity autocorrelation function of acute brain tissue slices from rats and examine the relationship between the characteristic decorrelation time and tissue thickness, comparing the results with the theoretical predictions of diffusing wave spectroscopy (DWS) which suggest that the decorrelation time should be inversely proportional to the square of the thickness [8–12]. The results of this study elucidate the time scale on which the movement inside tissue occurs and guide the further development of fast wavefront shaping techniques, especially toward the development of improved light delivery techniques for optogenetics both on *in vitro* acute brain slices and eventually for *in vivo* applications [13–16].

2. THEORY

The wave nature of light allows for very small changes in optical path length to be probed using interference. In samples which exhibit strong multiple scattering such as biological tissue, these interference effects manifest themselves as a speckle pattern and changes to the scattering media cause the speckle pattern to

change over time. By capturing a sequence of images of the speckle pattern over time, the degree of correlation between a reference frame and each subsequent frame can be computed, thus providing a measure of how rapidly the scatterers inside the sample are moving. This method of measuring the intensity correlations of speckle over time to analyze the dynamic nature of scattering media was originally developed by Maret, Wolf, Pine, and others in the late 1980s and is known as DWS [8,10,17].

The main aim of DWS is to relate the movement of the scatterers to the decay of the autocorrelation of the measured electric field. As derived by Maret and Wolf [17], the electric field autocorrelation in the case of multiple scattering and Brownian motion particle diffusion can be written as

$$g_1(\tau) = \int_0^\infty P(s) \exp\left[\left(-\frac{2\tau}{\tau_0}\right)\frac{s}{l^*}\right] \mathrm{d}s, \tag{1}$$

where τ is the delay time, $\tau_0 = 1/(Dk_0^2)$ is the characteristic decay time, $k_0 = 2\pi/\lambda$ is the wavenumber of the light in the medium, D is the diffusion constant of the scattering particles, l^* is the transport mean-free path, s is the path length, and $P(s)$ is the distribution of path lengths in the medium. From this equation we can see that the field autocorrelation is essentially a weighted sum [weights $P(s)$] of exponential decays at rates set by D, k_0, l^*, and s. However, by examining different thicknesses of the same sample in the same experimental configuration, D, k_0, and l^* are essentially fixed. Therefore, we can directly probe the relationship between the thickness and the characteristic decay time by determining the dependence of $P(s)$ on the thickness.

By measuring the ratio of unscattered light to the incident beam intensity, we found the scattering coefficient for the brain slices in our experiment to be $\mu_s = 50/\mathrm{mm}$. This is in good agreement with the values found in the literature [18]. Using this fact and the forward scattering nature of tissue (anisotropy factor of $g \approx 0.9$), we find a reduced scattering coefficient of $\mu_s' \approx 5/\mathrm{mm}$. We note here that in our experiment we assume that absorption is negligible since the mean absorption length is an order of magnitude longer than the transport mean-free path ($\mu_a = 0.2/\mathrm{mm}$, $\mu_s' = 5/\mathrm{mm}$) [10,18,19]. If the sample thickness is much greater than the transport mean-free path ($L \gg l^*$), the transport of light can be treated as diffusive. Under this assumption, commonly known as the diffusion approximation, DWS theory predicts via a first cumulant expansion of the electric field autocorrelation function that the decay of the autocorrelation function [Eq. (1)] should be proportional to $1/L^2$, where L is the sample thickness [8]. However, when the sample thickness is thin enough so that it is only several times greater than the transport mean-free path, the predictions of the diffusion approximation will break down and the decay of the autocorrelation will be more closely proportional to $1/L$, due to the quasi-ballistic propagation of light [20–23]. Here we note that even if the diffusion approximation is not valid, the framework of DWS still holds as long as the light is multiply scattered by noninteracting Brownian particles [17]. In practice, the path length distribution $P(s)$ in cases where the diffusion approximation breaks down is difficult to analytically calculate and must be approximated via computational methods such as Monte Carlo analysis.

In order to experimentally measure the electric field autocorrelation function it would be most convenient to directly measure the electric field of the scattered light field. However, due to the limitations of intensity-only detectors such as photodiodes and conventional CMOS and CCD cameras, measuring the electric field directly is not experimentally convenient. Fortunately, using intensity-only measurements we can calculate an intensity autocorrelation function by comparing data points taken at time t_0 and at a later time $t_0 + \tau$ and relate the calculated intensity autocorrelation function to the electric field autocorrelation function via the Siegert relation [24]. Here, the intensity autocorrelation function is given by

$$g_2(\tau) \equiv \frac{\langle I(t_0) I(t_0+\tau)\rangle}{\langle I(t_0)\rangle \langle I(t_0+\tau)\rangle}, \tag{2}$$

where $I(t_0)$ and $I(t_0 + \tau)$ are the captured intensities at times t_0 and $t_0 + \tau$, respectively, and $\langle\cdot\rangle$ indicates an average over all captured data for a given delay time. Then, assuming an ergodic system, the intensity autocorrelation function can be related to the field autocorrelation function through the Siegert relation as

$$g_2(\tau) = 1 + \beta |g_1(\tau)|^2. \tag{3}$$

Here, $g_2(\tau)$ is the intensity autocorrelation function, $g_1(\tau)$ is the field autocorrelation function, and β is an experimental factor between 0 and 1 determined by the collection optics and capture parameters. In our experiment, β is determined to be ~0.7–0.8 by using the value $\beta = g_2(0) - 1$.

Traditionally, the intensity autocorrelation function is calculated by monitoring the intensity fluctuations of a single speckle via a photodiode and relating the intensity autocorrelation to the field autocorrelation function using ergodicity. However, with the recent advances in high-speed camera technology along with improved data storage and transfer speed capabilities, a more powerful experimental scheme is available. In multispeckle diffusing wave spectroscopy, the photodiode is replaced by a high-speed array sensor which samples many speckles in parallel at the same time [11]. This relaxes the requirements for temporal ergodicity of the sample since many speckles are measured in parallel and enhance the statistical strength of the method to analyze systems with both fast and slow dynamics. In this framework, each measurement is a 2D image, the multiplication in Eq. (2) is computed elementwise, and the temporal averages are replaced by pixelwise averages of the stationary 2D captured frames. Using this procedure, we can capture a time series of speckle pattern images generated by the scattering media and compute the field autocorrelation function [$g_1(\tau)$] using the intensity autocorrelation function [$g_2(\tau)$] and the Siegert relation [Eq. (3)], thereby characterizing the dynamic nature of the sample.

3. EXPERIMENTAL SETUP

Figure 1 shows a diagram of the experimental setup used to capture the sequence of speckle patterns. A diode-pumped solid state laser ($\lambda = 532$ nm) illuminates the bottom surface of the sample rat brain slice with a beam diameter of approximately 500 μm. The brain slice is gently fixed with a slice anchor (Warner Instruments, SHD-22L/15) at room temperature in

a homemade bath containing phosphate buffered saline to keep the sample hydrated and at a constant temperature. The speckle patterns were captured using a microscope objective focused on the top surface of the brain tissue (Olympus, 20X LCAch N PH) and imaged to a sCMOS camera (PCO-TECH, pco.edge 5.5) at a frame rate of 100 frames per second and exposure time of 1 ms. To improve the contrast of the captured speckle images, a linear polarizer was placed in the infinity space region of the microscope and an iris was placed directly behind the exit pupil of the objective to control the speckle size on the detector. The iris was set such that the speckle size on the camera was $\sim 3 \times 3$ pixels to ensure adequate sampling [11]. In order to sample a large number of speckles for statistical stability, a 200×200 pixel region of interest in the center of the frame was selected ($\sim$4400 speckles). The entire setup was firmly mounted on a vibration isolating optical table to ensure stability and confirmed using a static scattering sample.

Four brain tissue thicknesses of 1, 1.5, 2, and 3 mm from a 3 month old Long–Evans rat were sliced using a vibratome (Leica, VT1200) to ensure accurate thickness. All animal handling procedures were conducted in compliance with the Institutional Animal Care and Use Committee at the California Institute of Technology. Then, the brain tissue slices were mounted in the tissue holder and speckle patterns were captured from $\sim$12 different positions in the tissue samples. The data was captured as quickly as possible within a period of several hours following acquisition of the slices to ensure maximum sample freshness.

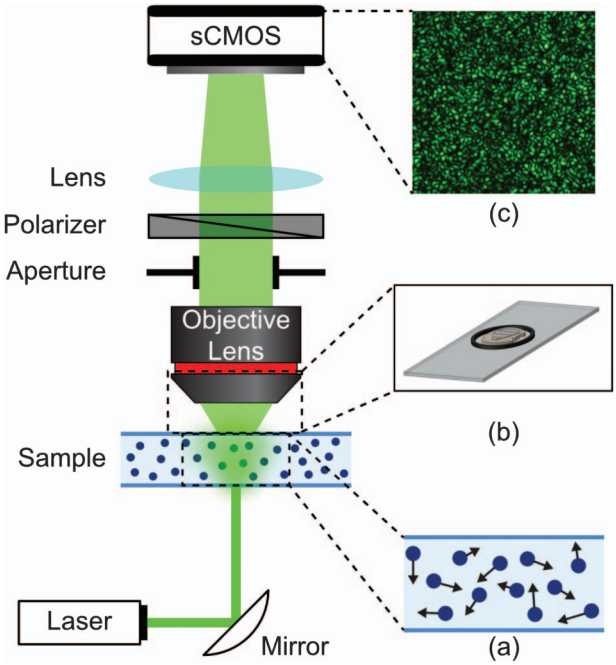

Fig. 1. Experimental setup used to capture the speckle patterns. (a) The scatterers inside the tissue cause the collimated light to form a diffusive speckle pattern which changes over time due to the random Brownian motion of the scatterers within the tissue. (b) Diagram illustrating how the sample is mounted. (c) The speckle pattern is then imaged on the camera and a sequence of images is captured.

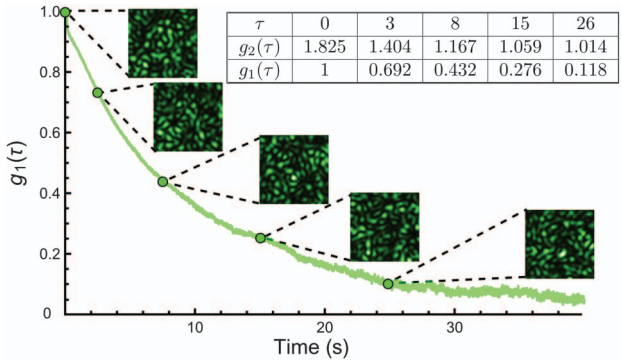

Fig. 2. Calculation procedure for calculating the decorrelation curves is performed by comparing each speckle pattern in the captured sequence with an original reference frame ($\tau = 0$). By pixelwise multiplying the sample and reference speckle image together and dividing by the mean intensities of each image, the degree of correlation at delay time τ can be quantified as $g_2(\tau)$. Then, $g_1(\tau)$ is calculated via Eq. (3).

4. DATA ANALYSIS

After a time series of speckle images is captured, the image stacks are analyzed in MATLAB according to Eq. (2) to compute the intensity autocorrelation function for each thickness. Figure 2 shows an intuitive way to understand the calculation procedure.

The images in Fig. 2 represent the captured speckle patterns at delay times of 0, 3, 8, 15, and 26 s, respectively. In order to compute the intensity correlation function $g_2(\tau)$, each image in the time series is multiplied entrywise with the first image in the series, and the pixelwise average of this product is divided by the product of the pixelwise averages of individual frames. Then, the Siegert relation is used to calculate the field autocorrelation function, where β is taken as $g_2(0)$ to normalize $g_1(\tau)$.

5. EXPERIMENTAL RESULTS

In order to analyze the relationship between the decay rate of the decorrelation curves and the thickness of the sample, we fit each individual decorrelation curve to an exponential decay function given by

$$a * \exp\left(-\frac{t}{t_d}\right) + (1 - a), \tag{4}$$

where a is the amplitude of the decay, the $(1 - a)$ offset is added to account for noise factors which cause the decorrelation function not to drop to zero as $t \to \infty$, and t_d is the decorrelation time. Here, the decorrelation time t_d is inversely related to the first cumulant, providing a measure of the average decay rate of the distribution [25]. Therefore, by fitting the decorrelation curves in this way and calculating the decorrelation time we can provide a figure of merit for the decay of the autocorrelation function and the movement of the scatterers in the tissue.

Figure 3 shows the decorrelation curves for the 1.0, 1.5, 2.0, and 3.0 mm rat brain tissue slices. Each plot shows the fitted curve of the sample mean across trials with dashed fitted curves above and below indicating the sample standard deviation of the curves. As the tissue sample thickness increases, the decay rate of the decorrelation curves increases.

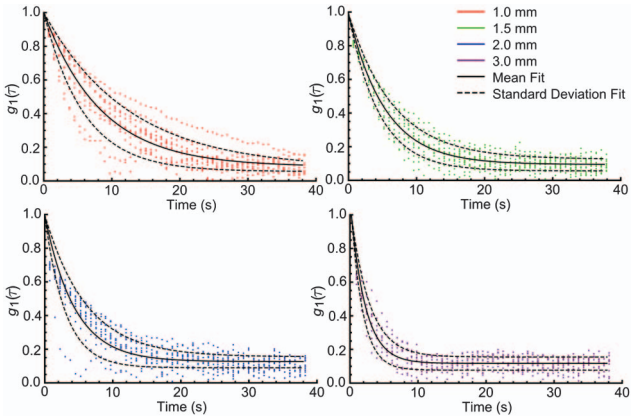

Fig. 3. Decorrelation curves for 1.0, 1.5, 2.0, and 3.0 mm thick brain slices. Data points shown at intervals of 0.75 s. 12, 13, 12, and 10 data sets are presented for the 1.0, 1.5, 2.0, and 3.0 mm thicknesses, respectively. The center of the three fitted curves show the sample mean and the two outer curves show the sample standard deviation bounds.

Figure 4 shows the decorrelation times of each trial with respect to the tissue thickness. This decorrelation time indicates the time it takes for the amplitude (a) of the calculated electric field autocorrelation function to decay to a/e. The measured data show an average decorrelation time of 9.38, 5.65, 3.95, and 2.27 s with standard deviations of 3.63, 1.50, 1.03, and 0.89 s for the 1.0, 1.5, 2.0, and 3.0 mm thicknesses, respectively. To analyze the trend of the decorrelation time versus tissue thickness, we fit the decorrelation time data with a model related to the inverse of a power of the tissue thickness L, $f(L) = a/L^b$. This yields fitted values of $a = 9.40$ and $b = 1.26$. As we expected, we see that the relationship between the decorrelation time and tissue thickness falls between a $1/L$ and $1/L^2$ description.

There are several reasons why the relationship between decorrelation time and thickness is not purely described by a $1/L$ or $1/L^2$ model. The first reason is due to the breakdown of the diffusion approximation. As noted by several authors in the DWS community, the assumption that light can be treated as diffusive begins to break down in the regime where the thickness of the scattering medium is of the same order of magnitude as the transport mean-free path ($L < 10 \times l^*$) [20–23]. In fact, when the scattering medium is only a few times thicker than the transport mean-free path, the actual scattering path length distribution $P(s)$ is skewed toward shorter path lengths than predicted by photon-diffusion approximation [22]. This is due to the fact that while the diffusion approximation suggests that the path lengths increase proportional to the square of the thickness of the scattering medium, the scattering path length of the quasi-ballistic component linearly scales with the sample thickness, resulting in a $1/L$-scaling of the decorrelation time [21]. As mentioned earlier, the transport mean-free path in the gray matter of rat brain used in this experiment is ~0.2 mm. Thus, in the thickness range from 1 to 3 mm, we expect to observe the transition in scaling relation between a $1/L$ model toward a $1/L^2$ model rather than the exact $1/L^2$ scaling predicted by the diffusion approximation. In addition, while the order of magnitude difference between the mean absorption length and the mean scattering length decreases the effect of absorption, incorporating the effects of absorption also shifts the characteristic decay times toward a $1/L$ model even in the diffusive regime [10]. This discussion is continued in Section 6, where we perform Monte Carlo simulations to analyze the effect of sample thinness (nondiffusive regime) and absorption.

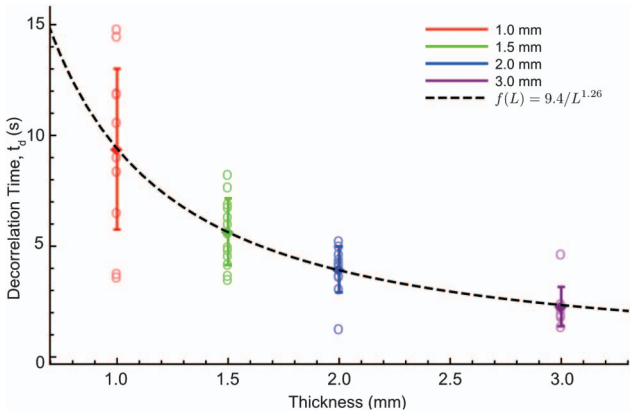

Fig. 4. Decorrelation times of the individual trials plotted with respect to the tissue thickness. The mean decorrelation curve is indicated by the solid line with sample standard deviation bounds illustrated by the dashed lines above and below.

While our experiment was designed to reduce the influence of potential sources of experimental error, the unavoidable heterogeneity of the sample leads to spatially varying scattering properties, therefore impacting the decay characteristics. These effects are especially pronounced in the thin slices (1.0 and 1.5 mm) where the transport mean-free path is especially small compared to the thickness. This means that even small changes in the transport mean-free path will have a significant impact on the path length distribution [$P(s)$] and ultimately on the decay characteristic of the tissue.

6. MONTE CARLO SIMULATION

To further investigate the sources for the deviation from the $1/L^2$ prediction of the diffusion approximation, we conducted a Monte Carlo simulation of the photon transport through the tissue to evaluate the path length distribution $P(s)$ of the photons traveling through the sample. Modeling the sample as a semi-infinite slab medium with the optical properties $\mu_s = 50/\text{mm}$, $g = 0.9$, and $\mu_a = 0.2/\text{mm}$, we simulated the path length distributions for the 1, 1.5, 2, and 3 mm thicknesses used in our experiment. To construct the path length distributions we built a custom single-layer, time-resolved Monte Carlo simulation based on the standard Monte Carlo simulation package developed by Wang *et al.* [26], recording the path length of each photon which passed through the sample and was collected within the 0.2 NA and ~0.2 mm^2 field of view of the objective used. The results of the Monte Carlo simulation are shown below in Fig. 5.

As the thicknesses of the sample increase, we observe a growing average path length as well as a broadening of the path length distribution. For the 1.0, 1.5, 2.0, and 3.0 mm slices, the average path lengths are 2.1, 3.9, 5.8, and 10.2 mm,

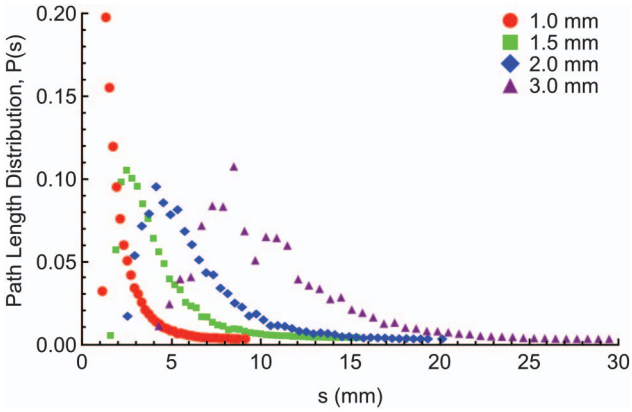

Fig. 5. Results of the Monte Carlo simulation of 1×10^6 photons with tissue properties $\mu_s = 50/\text{mm}$, $\mu_a = 0.2/\text{mm}$, and $g = 0.9$. The plot shows the path length distribution $P(s)$ versus path length s for 1.0, 1.5, 2.0, and 3.0 mm thick samples. As the tissue thickness increases, the mean path length increases and the distribution broadens.

respectively. Since the first cumulant expansion exponential fits used to determine the decorrelation times are proportional to the inverse of the mean path length, we can analyze the relationship between the inverse of the mean path length and thickness to get a better understanding of the relationship between decorrelation time and thickness from the simulation results. Figure 6 shows the relationship between the inverse of the mean path length and the tissue thickness both in the cases where absorption is present and when it is not.

From the simulated data points and corresponding fits in Fig. 6 we can understand the influence of absorption on the measured results. Plotting the inverse of the mean path lengths with respect to tissue thickness and fitting with a/L^b, where a and b are fitting parameters and L is the tissue thickness, reveals that the effect of absorption at small thicknesses is to shift the trend of the decorrelation curve from a $1/L^2$ relationship toward a $1/L$ trend. For the tissues greater than 2.0 mm we see that the absorption plays a role by terminating the long scattering path lengths, thereby reducing the mean scattering path length. These results suggest that the absorption of the tissue, while much weaker than the effects of scattering, still has a marked impact on the trend of decorrelation time versus thicknesses, reducing the strength of the $1/L^x$ trend.

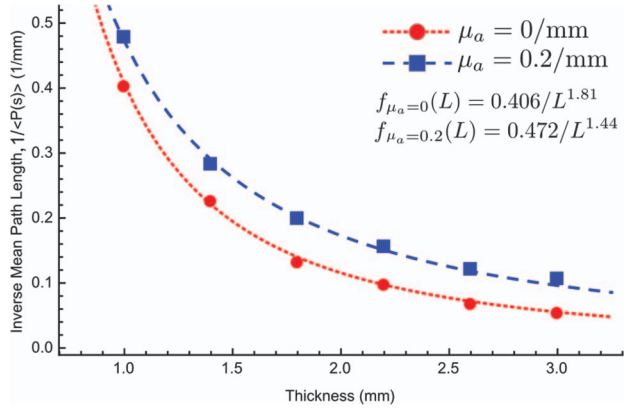

Fig. 6. Inverse mean path length $\langle P(s) \rangle$ versus sample thickness for 1–3 mm. The fitted curves (dashed lines) show the corresponding fits of a/L^b. Here we can clearly see that the effect of absorption both decreases the mean path length and slows the decay from being proportional to $1/L^{1.81}$ to $1/L^{1.44}$.

7. CONCLUSION

In this paper we have experimentally probed the relationship between the decorrelation time and the thickness of rat brain tissue using multispeckle diffusing wave spectroscopy. As new optical tools are developed to focus light deep into brain tissue for imaging or selective excitation of neuronal populations, these results will serve as a useful guide in determining how fast these systems must be to respond to the dynamic nature of tissue in the absence of blood.

We note that in general, the movement of blood and surrounding tissues causes much faster decorrelation and is the ultimate challenge to overcome in *in vivo* applications. However, the results of this study are directly applicable to the selective excitation of neurons in acute brain slices via optogenetics using deep-tissue light-focusing methods and also to *in vivo* experiments where blood flow is suppressed via immobilization techniques [7].

Recently, several fast wavefront shaping techniques have been demonstrated with response speeds of the order of several milliseconds [14,15]. Based on the results from this study, we expect that these wavefront shaping techniques will be able to successfully focus light through brain tissue thicker than 10 mm as long as certain practical SNR requirements are met. This capability may enable entire acute brain sections to be optogenetically excited using these techniques. In future studies we hope to investigate further how this information can enhance the development of novel optical systems to overcome the dynamic nature of biological tissue and enable *in vivo*, deep-tissue imaging.

Funding. National Institute of Biomedical Imaging and Bioengineering (NIBIB) (1F31EB021153-01); National Institute of Neurological Disorders and Stroke (NINDS) (1U01NS090577-01); National Institutes of Health (NIH) (1DP2OD007307-01); Donna and Benjamin M. Rosen Bioengineering Center; GIST-Caltech (CG2012).

Acknowledgment. J. B. acknowledges support from an NIH NRSA Predoctoral Fellowship and the Donna and Benjamin M. Rosen Bioengineering Center. The authors would also like to thank Dr. Cheng Xiao for his help in preparing the brain tissue slices.

†These authors contributed equally to this work.

REFERENCES

1. J. W. Goodman, *Speckle Phenomena in Optics: Theory and Applications* (Roberts & Company, 2007).
2. A. P. Mosk, A. Lagendijk, G. Lerosey, and M. Fink, "Controlling waves in space and time for imaging and focusing in complex media," Nat. Photonics **6**, 283–292 (2012).

3. I. M. Vellekoop and A. Mosk, "Focusing coherent light through opaque strongly scattering media," Opt. Lett. **32**, 2309–2311 (2007).
4. R. Horstmeyer, H. Ruan, and C. Yang, "Guidestar-assisted wavefront-shaping methods for focusing light into biological tissue," Nat. Photonics **9**, 563–571 (2015).
5. X. Xu, H. Liu, and L. V. Wang, "Time-reversed ultrasonically encoded optical focusing into scattering media," Nat. Photonics **5**, 154–157 (2011).
6. Y. M. Wang, B. Judkewitz, C. A. DiMarzio, and C. Yang, "Deep-tissue focal fluorescence imaging with digitally time-reversed ultrasound-encoded light," Nat. Commun. **3**, 928 (2012).
7. M. Jang, H. Ruan, I. M. Vellekoop, B. Judkewitz, E. Chung, and C. Yang, "Relation between speckle decorrelation and optical phase conjugation (OPC)-based turbidity suppression through dynamic scattering media: a study on in vivo mouse skin," Biomed. Opt. Express **6**, 72–85 (2015).
8. D. Pine, D. Weitz, P. Chaikin, and E. Herbolzheimer, "Diffusing wave spectroscopy," Phys. Rev. Lett. **60**, 1134–1137 (1988).
9. F. MacKintosh and S. John, "Diffusing-wave spectroscopy and multiple scattering of light in correlated random media," Phys. Rev. B **40**, 2383–2406 (1989).
10. D. Pine, D. Weitz, J. Zhu, and E. Herbolzheimer, "Diffusing-wave spectroscopy: dynamic light scattering in the multiple scattering limit," J. Phys. France **51**, 2101–2127 (1990).
11. V. Viasnoff, F. Lequeux, and D. Pine, "Multispeckle diffusing-wave spectroscopy: a tool to study slow relaxation and time-dependent dynamics," Rev. Sci. Instrum. **73**, 2336–2344 (2002).
12. D. Weitz, J. Zhu, D. Durian, and D. Pine, "Principles and applications of diffusing-wave spectroscopy," in *Structure and Dynamics of Strongly Interacting Colloids and Supramolecular Aggregates in Solution* (Springer, 1992), pp. 731–748.
13. K. Deisseroth, "Optogenetics," Nat. Meth. **8**, 26–29 (2011).
14. D. Wang, E. H. Zhou, J. Brake, H. Ruan, M. Jang, and C. Yang, "Focusing through dynamic tissue with millisecond digital optical phase conjugation," Optica **2**, 728–735 (2015).
15. Y. Liu, P. Lai, C. Ma, X. Xu, A. A. Grabar, and L. V. Wang, "Optical focusing deep inside dynamic scattering media with near-infrared time-reversed ultrasonically encoded (TRUE) light," Nat. Commun. **6**, 5904 (2015).
16. D. B. Conkey, A. M. Caravaca-Aguirre, and R. Piestun, "High-speed scattering medium characterization with application to focusing light through turbid media," Opt. Express **20**, 1733–1740 (2012).
17. G. Maret and P. Wolf, "Multiple light scattering from disordered media. The effect of Brownian motion of scatterers," Z. Phys. B **65**, 409–413 (1987).
18. M. Azimipour, R. Baumgartner, Y. Liu, S. L. Jacques, K. Eliceiri, and R. Pashaie, "Extraction of optical properties and prediction of light distribution in rat brain tissue," J. Biomed. Opt. **19**, 075001 (2014).
19. M. Mesradi, A. Genoux, V. Cuplov, D. A. Haidar, S. Jan, I. Buvat, and F. Pain, "Experimental and analytical comparative study of optical coefficient of fresh and frozen rat tissues," J. Biomed. Opt. **18**, 117010 (2013).
20. D. Durian, "Accuracy of diffusing-wave spectroscopy theories," Phys. Rev. E **51**, 3350–3358 (1995).
21. I. Freund, M. Kaveh, and M. Rosenbluh, "Dynamic multiple scattering: ballistic photons and the breakdown of the photon-diffusion approximation," Phys. Rev. Lett. **60**, 1130–1133 (1988).
22. K. Yoo, F. Liu, and R. Alfano, "When does the diffusion approximation fail to describe photon transport in random media?" Phys. Rev. Lett. **64**, 2647–2650 (1990).
23. P.-A. Lemieux, M. Vera, and D. Durian, "Diffusing-light spectroscopies beyond the diffusion limit: the role of ballistic transport and anisotropic scattering," Phys. Rev. E **57**, 4498–4515 (1998).
24. P.-A. Lemieux and D. J. Durian, "Investigating non-Gaussian scattering processes by using nth-order intensity correlation functions," J. Opt. Soc. Am. A **16**, 1651–1664 (1999).
25. B. J. Frisken, "Revisiting the method of cumulants for the analysis of dynamic light-scattering data," Appl. Opt. **40**, 4087–4091 (2001).
26. L. Wang, S. L. Jacques, and L. Zheng, "MCML—Monte Carlo modeling of light transport in multi-layered tissues," Comput. Meth. Programs Biomed. **47**, 131–146 (1995).